Received: 19 May 2021 | Revised: 24 September 2021 | Accepted: 27 September 2021

DOI: 10.1002/app.51777

ARTICLE

Applied Polymer SCIENCE WILEY

Porphyrin cross-linked conjugated polymer nanoparticles-based photosensitizer for antimicrobial and anticancer photodynamic therapies

Ishmeal Kwaku Duah[1] | **Aisan Khaligh**[1,2] | **Ahmet Koç**[1] | **Duygu Deniz Akolpoğlu Başaran**[2] | **Dönüs Tuncel**[1,2]

[1]Department of Chemistry, Bilkent University, Ankara, Turkey

[2]Institute of Materials Science and Nanotechnology, National Nanotechnology Research Center (UNAM), Bilkent University, Ankara, Turkey

Correspondence
Dönüs Tuncel, Department of Chemistry, Bilkent University, 06800 Ankara, Turkey.
Email: dtuncel@fen.bilkent.edu.tr

Abstract

We report here the synthesis and characterization of a water dispersible conjugated polymer nanoparticle-based photosensitizer and its application in the antibacterial and anticancer phototherapies. Nanoparticles (**CPPN**) were synthesized in one-pot by nanoprecipitation method, in which a hydrophobic azide functionalized, red-emitting thiophene-benzothiodiazole based conjugated polymer (**CP-AZ**) was cross-linked with a hydrophilic, propargylamine functionalized porphyrin (**TPP-4AL**) through cucurbit[6]uril (**CB6**) catalyzed azide-alkyne cycloaddition (**CB6**-AAC) reaction. **CPPN** demonstrated high stability in aqueous medium for more than a month without any visible aggregation and appeared to be a good photosensitizer with high light-triggered reactive oxygen species (ROS) generation ability. Consequently, **CPPN** displayed photo-induced biocidal activity against Gram-negative (*Escherichia coli*, *E. coli*) and Gram-positive (*Bacillus subtilis*, *B. subtilis* and *Staphylococcus aureus*, *S. aureus*) bacteria. When bacteria suspension was incubated with **CPPN** (20 μg ml^{-1}) and irradiated with white light (22 mW cm^{-2}) for 10 min, more than 3.5-log reduction in colony-forming units (CFUs) was recorded for the three model bacteria. **CPPN** demonstrated minimal dark cytotoxicity against the bacteria. Moreover, the cytotoxicity of **CPPN** on mammalian cell was studied using MCF-7 breast cancer cell line. The results demonstrated that **CPPN** is non-toxic to mammalian cells in the dark even at a high concentration of 112.5 μg ml^{-1} and this feature makes **CPPN** an ideal photosensitizer.

KEYWORDS

biomedical applications, conducting polymers, drug delivery systems, nanocrystals, nanoparticles, nanowires, optical properties

1 | INTRODUCTION

Over the past decades, antibiotics have played an important role in the fight against pathogenic microorganisms and in prolonging human life. However, the abuse and overuse of antibiotics lead to the emergence of microbial strains resistant to antibiotics, making antimicrobial therapy a difficult problem. Eliminating the risk of antibiotic resistance is essential, and alternative antimicrobial treatments have been urgently sought to alleviate the crisis.[1]

To prevent the emergence of drug resistance and the controlled elimination of pathogens and cancer, photodynamic therapy (PDT) as an effective method was developed.[2] PDT is the photochemistry-based method that has been clinically approved due to its minimal invasiveness and side effects compared to other conventional therapies. Herein, three key elements for PDT include photosensitizer, light source, and molecular oxygen.[3] Ideal photosensitizers have good aqueous solubility and stability, minimal dark toxicity, and effective singlet oxygen ($^1O_2$) generation ability, where they can produce reactive oxygen species (ROS) upon exciting them at particular wavelengths of light. ROS interacts with many cellular components through oxidative reactions. As a result, the activity of cells, is disrupted, leading to cell death. Herein, ROS kill the bacteria by damaging cell membranes, leading to leakage of cellular contents, which inactivates the enzymes and turns off their membrane transport system.[3]

In this regard, porphyrin and its derivatives have attracted a great deal of attention to use as potential photosensitizers in PDT, due to their planar aromatic structure, remarkable photophysical properties, efficient absorption of visible red light, long-living triplet excited state, high molar extinction coefficient and high ROS yield upon irradiation with light.[4] Moreover, their synthetic versatility, easily functional modification and structural diversity, chemical stability and flexibility facilitate the development of multifunctional assemblies with potential applications in biomedicine. To date, many porphyrin derivatives, such as Photofrin® and Fotolon® have been approved for clinical use by health organizations.[4c,5] However, they still face many challenges, like low biocompatibility and less selectivity toward cancer cells. To enhance the therapeutic effects of PDT, the synthesis of novel and superior photosensitizers with excellent ROS generation ability and biocompatibility is needed.[4c,5]

Nanomaterial-based systems are also gaining an increasing attention because they can hold many functionalities including the photoactive units, drugs, and targeting groups in one platform to fight infectious diseases and cancer more effectively.[6] Recently, conjugated polymer (CP)-based nanostructures started to emerge as an effective photosensitizer for the antibacterial and anticancer photodynamic therapies due to their unique electronic and optical properties exhibiting strong light-harvesting capability, high singlet oxygen generation ability, tunable optical spectrum, and many more.[7] While the basic optical properties of CPs are determined by the structure of the polymer backbone, side chains linked to backbone can be tailored easily by installing desired functional groups for the defined applications.[7e–h]

In this study, we combine conjugated polymers with porphyrins to obtain water dispersible and mechanically stable nanoparticles with an ability to generate singlet oxygen efficiently. All these features are highly sought after for an ideal photosensitizer. These conjugated polymer-porphyrin nanoparticles (**CPPN**) were synthesized in one pot by nanoprecipitation method by cross-linking a hydrophobic azide-functionalized conjugated polymer (**CP-AZ**) with a water- soluble propargylamine-functionalized porphyrin (**TPP-4AL**) through cucurbit[6]uril-(**CB6**)-catalyzed azide–alkyne cycloaddition (**CB6-AAC**) reaction.[8] Macrocycle **CB6** is one of the homologues of **CBn** family which contains six glycoluril ($n = 6$) units having a hydrophobic cavity and two hydrophilic portals each having six carbonyl groups.[9] It can encapsule suitably sized hydrophobic guests in its cavity and complex with cationic guests through ion-dipole interaction. CB6 can also catalyze 1,3-dipolar cycloaddition between alkyne and azide forming a triazole.[8] **CBn** homologues have been used extensively in the construction of nanostructured materials for a wide range of applications.[10] Here, we utilized **CB6** to link porphyrin units to the conjugated polymers for several reasons. Firstly, CB6 is used as a catalyst for alkyne-azide click reaction and in this way, the use of Cu(I) as a catalyst has been avoided as even residue of Cu can show toxicity for the biological applications.[10b] Secondly, hydrophilic groups are introduced to the NPs which render them highly water dispersible but due to the cross-linking also makes them stable by keeping them intact. Introduced cationic units are also important as they prevent NPs to coalesce due to the electrostatic repulsion and allow bacteria to interact with NPs more effectively.[10c–f] Thirdly, although the cationic head groups are known to cause dark toxicity, the presence of CB6 with coordinating with them, reduce their toxicity effects.[7j,10c–f] Accordingly, **CPPN** was used as a photosensitizer in PDT to study its killing ability toward Gram-negative (*E. coli*) and Gram-positive (*B. Subtilis* and *S. aureus*) bacteria. Moreover, the cytotoxicity of **CPPN** against MCF-7 breast cancer cell was investigated in the dark and under light irradiation.

2 | RESULTS AND DISCUSSION

2.1 | Synthesis and characterization of CP-AZ and CPPN

In order to prepare the porphyrin cross-linked conjugated polymer nanoparticles (CPPN), first azide functionalized conjugated polymer, **CP-AZ,** was synthesized by a Pd-catalyzed Suzuki coupling reaction between 3-(2-azidoethyl)-2,-5-dibromothiophene (**M3**) and 2,1,3-benzothiadiazole-4,7-bis (boronic acid pinacol ester). Scheme 1 shows the synthetic

details of the precursor monomers and **CP-AZ**. The synthesized monomers and **CP-AZ** were characterized using ^{1}H NMR, ^{13}C NMR and FT-IR techniques (Figures S1–S10). The weight-average molecular weight (M_w) and number-average molecular weight (M_n) of **CP-AZ** measured by GPC were found to be 24,100 and 22,300, respectively, with PDI of 1.082. The photophysical properties of **CP-AZ** were evaluated using UV–vis absorbance and fluorescence spectroscopy methods in THF (Figure S11). **CP-AZ** showed two major absorption peaks at 319 and 494 nm with an emission peak at 620 nm. The fluorescence quantum yield was measured to be about 18% in THF.

After detailed characterization of **CP-AZ**, next we prepared nanoparticles (**CPPN)** through **CB6**-catalyzed azide alkyne cycloaddition reaction (CB6-AAC) between **CP-AZ** and **TPP-4AL** in one pot using nanoprecipitation method.[10b] **TPP-4AL** and **CB6** were synthesized following the literature procedures.[8b,8e,8f] Scheme 2 shows the main steps involved in the synthesis of **CPPN**. First**, CB6** (4 equimolar) was dissolved in 0.1 M aqueous solution of HCl and **TPP-4AL** (1 equimolar) was added to this solution while stirring to get a homogenous solution. A solution of **CP-AZ** (4 equimolar) in THF was rapidly injected to the above solution and then sonicated for 1 h. The concentrations of **CP-AZ** and **TPP-4AL** were varied to prepare a series of nanoparticles to find out the most optimum concentrations which were determined as 2 mg:0.5 mg/ml for **CP-AZ**: **TPP-4AL**. The resulting mixture was left overnight at room temperature for the reaction to complete and then, THF was removed under reduced pressure to obtain stable, water dispersible nanoparticles. Dialysis was done against water using a 14 kDa cut-off regenerated cellulose membrane for 16 h to remove excess **CB6** and any unreacted porphyrins.

The synthesized **CPPN** was fully characterized using ^{1}H NMR, FT-IR, SEM, TEM, XPS, and DLS analyses. The synthesis of **CPPN** was first confirmed using FT-IR. Figure 1 compares FT-IR spectra of **CPPN** with **CP-AZ** and **TPP-4AL**. The appearance of the carbonyl stretching signal at 1726 cm^{-1}, and the disappearance of the alkyne stretching signals for C≡C at 2130 cm^{-1} and for —C≡C—H at 3285 cm^{-1} together with the decrease in the intensity of the azide signal at 2095 cm^{-1} in the FT-IR spectrum of the targeted **CPPN** in comparison with the **CP-AZ** and **TPP-4AL** confirmed the success of the **CB6**-

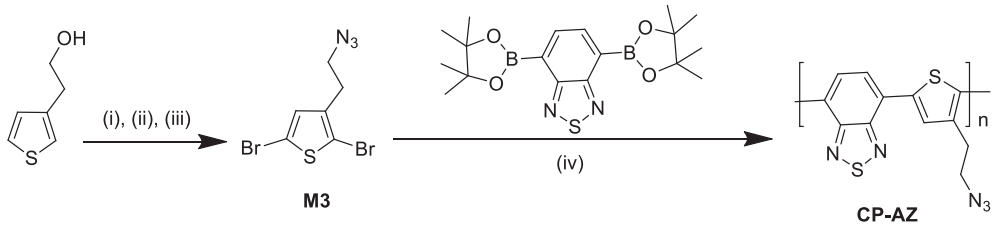

SCHEME 1 Synthetic routes for 2-(2,5-dibromothiophen-3-yl)ethan-l-ol (**M1**) and 2,5-dibromo-3-(2-bromoethyl)thiophene (**M2**) and **CP-AZ**: (i) **M1:** NBS, EtOAc, RT, overnight; (ii) **M2**: PPh_3, CBr_4, THF, RT, 24 h; (iii) **M3**: NaN_3, DMSO, RT, 72 h; (iv) **CP-AZ**: $Pd(PPh_3)_4$, TBAB, K_2CO_3, THF, toluene, H_2O, 55°C, 72 h, N_2

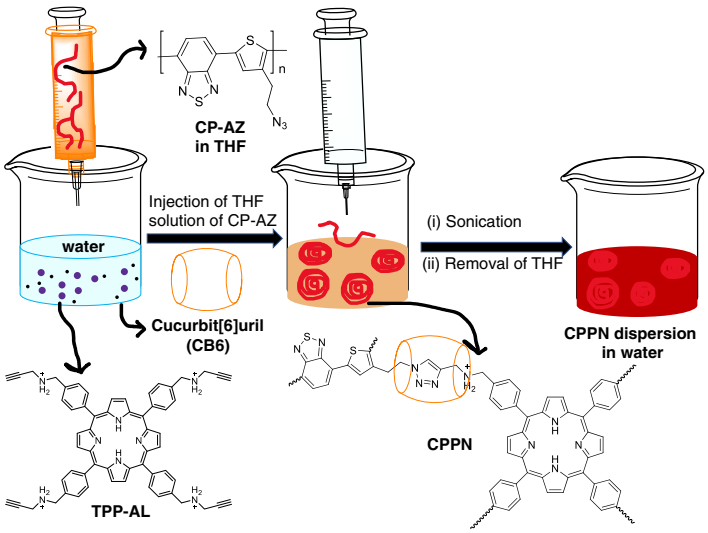

SCHEME 2 Schematic presentation of the **CPPN** preparation: **CB6** and **TPP-4AL** in 0.1 M HCl, CP-AZ in THF, RT, 1 h sonication [Color figure can be viewed at wileyonlinelibrary.com]

catalyzed click reaction. **CB6** does not only catalyze the click reaction by forming triazole that link together **CP-AZ** and **TPP-AL** but also remains as a part of the rotaxanated nanostructure. The rotaxane formation by the **CB6**-catalyzed click reaction initially involves the formation of a ternary complex between alkyne and azide functionalities as well as **CB6**. Correct alignment of azide and alkyne groups in the **CB6** cavity induces the formation of triazoles.[8] In order to take ^{1}H NMR, CPPN dispersion in water was concentrated under reduced pressure. The remaining solid residue was insoluble in any solvent as expected proving further the success of the cross-linking reaction. However, it was dispersed in DMSO-*d6* by stirring for overnight at RT and then its ^{1}H NMR spectrum was recorded. As shown in Figure S13, the ^{1}H NMR spectrum showed the characteristic signals of the protons of CB6, porphyrin, phenyl, and triazoles, hence further confirmed the success of **CB6**-AAC reaction to produce rotaxanes.

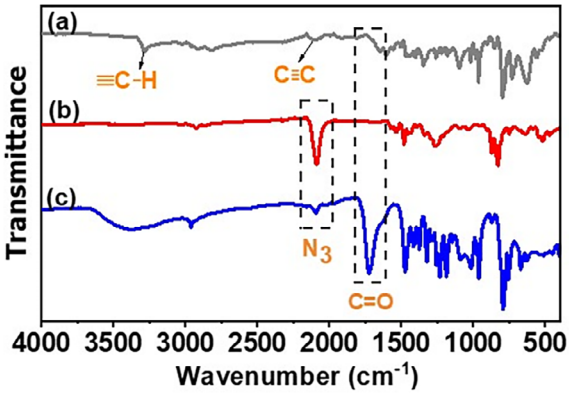

FIGURE 1 Comparison of FT-IR spectra of (c) **CPPN** with (a) **TPP-4AL** and (b) **CP-AZ** [Color figure can be viewed at wileyonlinelibrary.com]

The morphology of **CPPN** was studied using TEM and SEM (Figure 2a,b). Both TEM and SEM images revealed that **CPPN** are spherical in shape with smooth surface and average particle size around 150 nm. The SEM/EDX elemental mapping for the distribution of C, N, O, and S in the **CPPN** were presented in Figure 2c. The corresponding SEM/EDX spectrum and the atomic percentage of elements were given in Figure S14. Based on the SEM/EDX results, **CPPN** contains 51.46% C, 25.00% O, 23.32% N, and 0.22% S.

The elemental and chemical composition of **CPPN** was further evaluated with XPS analysis (Figure 3). The C1s XPS spectrum was fitted by seven components assigned to C═C (284.25 eV), C—C (284.70 eV), C-S (285.10 eV), C—N (285.41 eV), C—O (286.35 eV), C═O (287.62 eV), and N—C═O (289.10 eV). The N1s XPS spectrum was deconvoluted into three peaks assigned to C═N—C of pyrrolic-N and C═N—S of **CP-NZ** at 399.26 eV, amine-N and N—N═C of triazole-N and at 400.15 eV and $N(C)_3$ at 401.52 eV. The O 1s XPS spectrum presented a major peak at 532.25 eV assigned to C═O. The S2p core level XPS spectrum was fitted to four components with binding energies of 165.5 eV ($S2p_{3/2}$) and 166.7 eV ($S2p_{1/2}$) attributed to N—S—N bond[11] as well as 163.9 eV ($S2p_{3/2}$) and 165.1 eV ($S2p_{1/2}$) attributed to C—S—C bond.

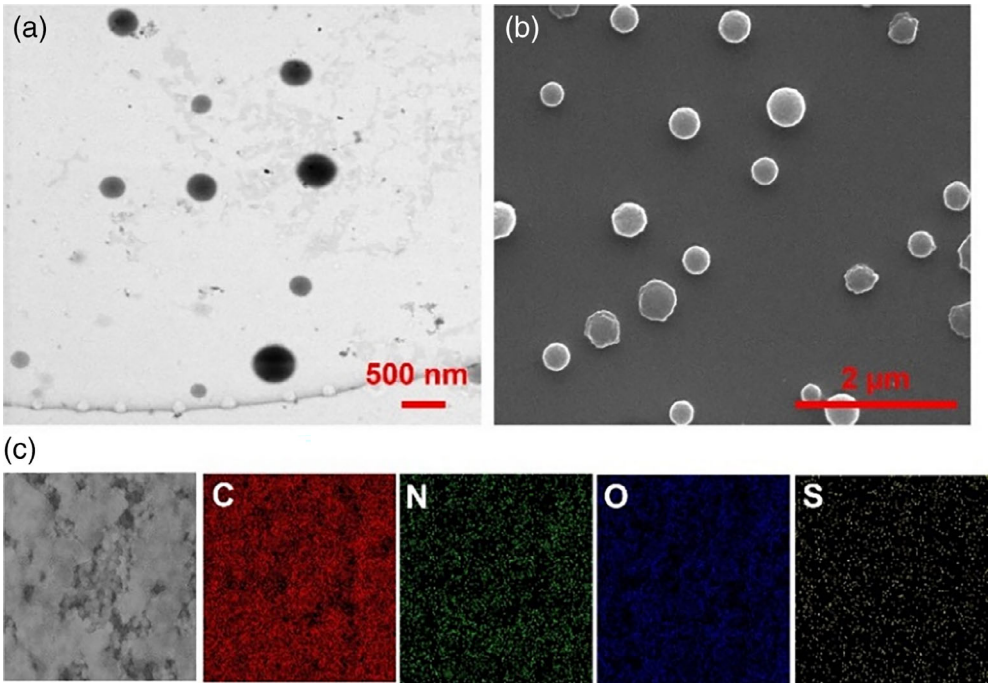

FIGURE 2 (a) TEM, (b) SEM, and (c) SEM/EDX elemental mapping images of **CPPN** [Color figure can be viewed at wileyonlinelibrary.com]

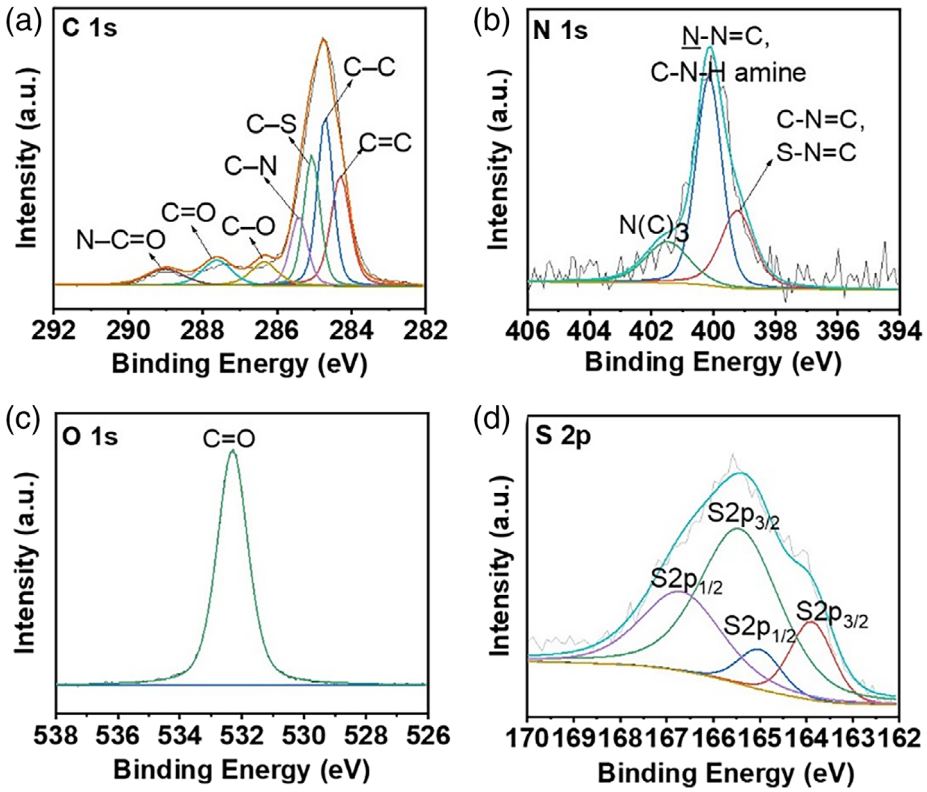

FIGURE 3 High resolution XPS data of **CPPN**: (a) C1S, (b) N1s, (c) O1s, and (d) S2p [Color figure can be viewed at wileyonlinelibrary.com]

The photophysical properties of **CPPN** were studied by UV–vis absorbance and fluorescence techniques (Figure S15). UV–vis measurement of **CPPN** displayed the major absorption peak at 415 nm assigned to Soret-band of porphyrin, a peak at 330 nm attributed to **CP-AZ** and some minor peaks at 519 nm, 555 nm and 592 nm assigned to Q-bands of **TPP-4AL**, which were mostly overlapped by the broad absorption peak of **CP-AZ** at 494 nm as shown in Figure S11. The fluorescence spectrum of **CPPN** showed two emission peaks at 650 nm and 705 nm.

The hydrodynamic size, polydispersity index (PDI) and surface charge (ζ-potential) of the **CPPN** were determined by DLS (Figure S16). The average hydrodynamic diameter and ζ-potential of **CPPN** were measured to be around 185 nm (with PDI value of 0.317) and +39 mV, respectively. (Figure S13). The ζ-potential of +39 mV indicates the good stability of **CPPN** in aqueous solution, while its positive value is due to the protonated amine functionalities of **TPP-4AL**. Moreover, the stability of **CPPN** in aqueous medium was monitored by measuring its average hydrodynamic diameter over the course of 36 days (200 μg ml^{-1}, RT). As shown in Figure S17, **CPPN** showed good stability in aqueous medium without any visible aggregation. The introduction of positive charges into the **CPPN** through the cross-linking, causes repulsion between the nanoparticles and prevents aggregation. In addition, the positive charges on **CPPN** can be served as binding sites toward the surface membrane of negatively charged surface bacteria.

2.2 | ROS generation ability of CPPN

The visible-light-induced ROS generation capability of **CPPN** was studied through the well-established DCFH-DA assay.[10c–f] Figure 4a represents the ROS detection mechanism of DCFH-DA assay. At first, NaOH aqueous solution hydrolysis DCFH-DA to DCFH. Then, in the presence of ROS, the non-fluorescent DCFH is quickly oxidized to fluorescent DCF with a clear increase in fluorescence intensity at 524 nm. The time responsive curves of DCFH oxidation in the blank solution without **CPPN** and in the presence of **CPPN**, under white light irradiation (1 mW cm^{-2}) were plotted in Figure 4b. The corresponding fluorescence spectra were shown in Figure 4c. From the results, the fluorescence intensity of DCF at 524 nm was remarkably increased in the presence of **CPPN** upon 4 min white light irradiation, while very small emission bands were recorded in the blank sample without **CPPN**. This confirmed the significant light-triggered ROS generation ability of **CPPN** even with relatively low light intensity.

2.3 | Broad spectrum photodynamic antibacterial activity of CPPN

The outstanding light-triggered ROS generation ability of **CPPN** encouraged us to investigate its visible light-induced antibacterial activity against *E. coli* (Gram-

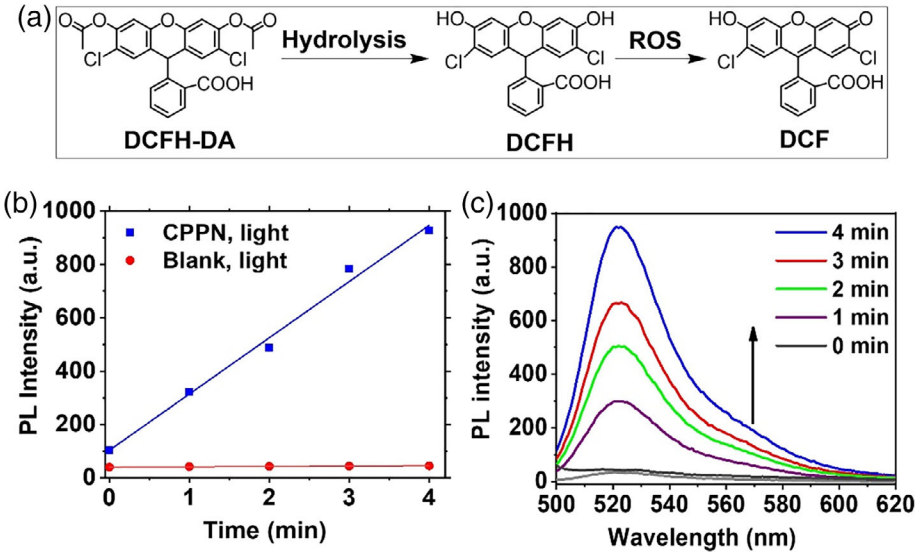

FIGURE 4 (a) Mechanism of ROS detection through DCFH-DA assay. (b) Time response curves of DCFH oxidation with and without **CPPN** under white light irradiation (1 mW cm^{-2}). (c) The corresponding fluorescence spectra of DCF at 524 nm in the presence of **CPPN**, under white light [Color figure can be viewed at wileyonlinelibrary.com]

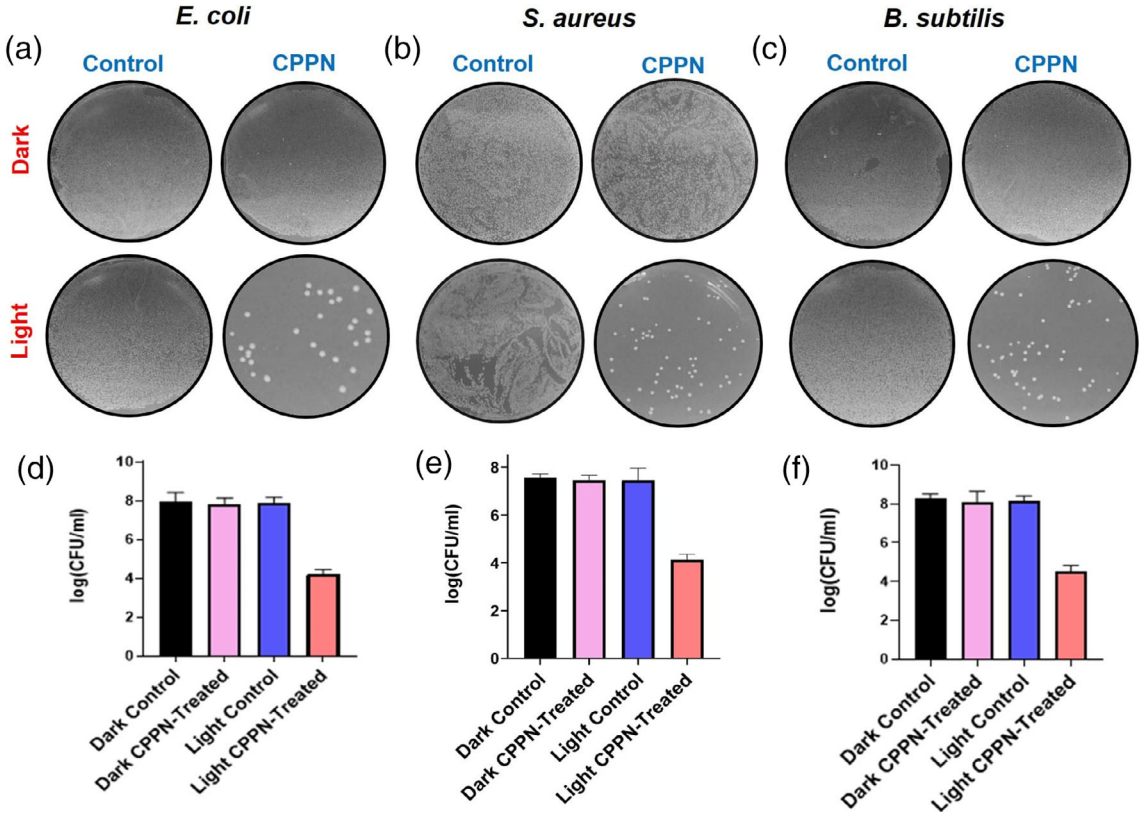

FIGURE 5 Plate photographs of bacteria: (a) *E. coli*, (b) *S. aureus*, and (c) *B. subtilis* for control and CPPN treated groups in the dark and under white light irradiation (22 mW cm^{-2}) for 10 min. The corresponding antibacterial activity of CPPN toward (d) *E. coli*, (e) *S. aureus*, and (f) *B. subtilis*. Results represent the mean ± SD of three separate experiments [Color figure can be viewed at wileyonlinelibrary.com]

negative), *B. subtilis* (Gram-positive), and *S. aureus* (Gram-positive) as three model bacteria. At first, the minimum inhibitory concentration (MIC) of **CPPN** was evaluated using broth dilution method to determine its optimum concentration.[12] To achieve this, 100 µl of *E. coli* suspension was treated with 10 µl of different concentrations of **CPPN** in the range of 5–30 µg ml^{-1}, both in the dark and under white light irradiation (22 mW cm^{-2}). Figure S18a,b displayed the effect of varying **CPPN** concentration on its antibacterial efficiency

toward *E. coli* in the dark and under light, respectively, in comparison with the control groups where the equal volume of PBS was used. From the results, with increasing **CPPN** concentration, its antibacterial efficiency was remarkably enhanced under white light irradiation and reached a plateau after 20 μg ml^{-1}. Therefore, MIC of **CPPN** toward *E. coli* was determined to be 20 μg ml^{-1}.

After this, bacterial suspensions were treated with 20 μg ml^{-1} of **CPPN** both in the dark and under white light irradiation (22 mW cm^{-2}) for 10 min and the bacterial killing ability of **CPPN** was estimated using surface plating method and the obtained results were presented in Figure 5a–f. Colony counting results demonstrated that around 3.8-log reduction in colony-forming units (CFUs) was achieved when *E. coli* was treated with 20 μg ml^{-1} of **CPPN** under white light irradiation for 10 min (Figure 5a). However, in the dark, **CPPN** shown almost no dark cytotoxicity. Also, about 3.6 and 3.5-log reduction in CFU was achieved for *B. subtilis* and *S. aureus*, respectively, when treated with 20 μg ml^{-1} of **CPPN** under 10 min light irradiation (Figure 5b,c). Therein, **CPPN** showed higher phototoxicity toward *E. coli* (Gram-negative) than the other two Gram-positive bacteria which can be attributed to the structural difference between Gram-positive and Gram-negative bacteria.

We have also prepared nanoparticles from **CP-AZ** in the absence of **TPP-4AL** and CB6 using nanoprecipitation method. DLS analysis revealed that the nanoparticles have a ζ-potential and an average hydrodynamic diameter of −30.7 mV and 67 nm, respectively (Figure S12). However, these nanoparticles appeared to be not suitable for the antibacterial experiments as they precipitated in the PBS. However, after cross-linking with **TPP-4AL** to produce **CPPN** no precipitation was seen.

Next, the photodynamic antibacterial activity of **CPPN** against *E. coli*, *B. subtilis*, and *S. aureus* was further evaluated using agar disk diffusion method, both in the dark and under white light irradiation (22 mW cm^{-2}) for 10 min, as described in Experimental section. Figure 6a–f compares the plate photographs of agar disk diffusion assay and the corresponding inhibition zone radius graphs of **CPPN** and ampicillin toward the three studied bacteria, both in the dark and under light conditions. The inhibition zone was determined by measuring the radius of the cell-free zone. As expected, the inhibition zone radius for ampicillin was around 7 mm for the three model bacteria, both in the dark and under light conditions. Meanwhile, almost no inhibition zone radius was seen for **CPPN** in the dark, however, its inhibition zone radius increased significantly under 10 min light illumination for the studied bacteria. This is in line with our previous observations using surface plating method. Overall, the remarkable photodynamic antibacterial efficacy of **CPPN** toward both Gram-positive and Gram-negative bacteria makes **CPPN** as a promising broad-spectrum antibacterial agent.

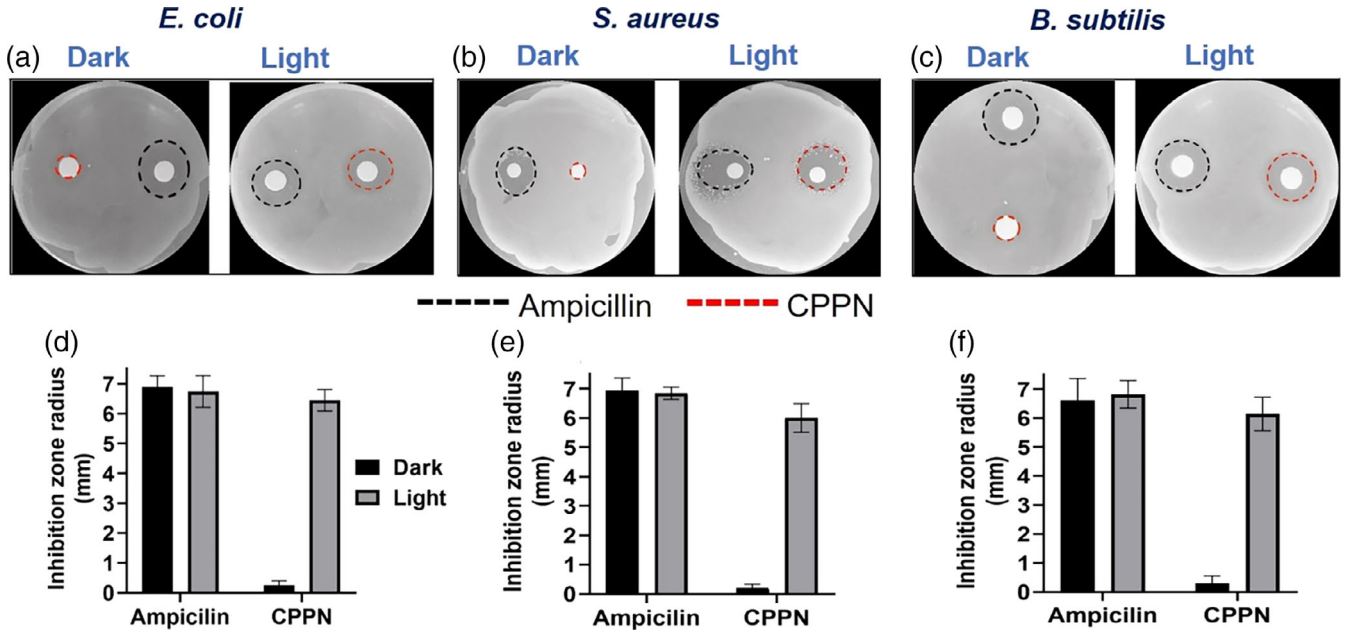

FIGURE 6 Plate photographs of agar disk diffusion assay of (a) *E. coli*, (b) *S. aureus* and (c) *B. subtilis*, treated with 20 μg ml^{-1} of **CPPN** and ampicillin in the dark and under white light irradiation (22 mW cm^{-2}) for 10 min. The corresponding inhibition zone radius graphs of (d) *E. coli*, (e) *S. aureus*, and (f) *B. subtilis*. The zone of inhibition is the average of the radii measured from at least six different spots on the circle. Results represent the mean ± SD of three separate experiments [Color figure can be viewed at wileyonlinelibrary.com]

2.4 | Investigation of CPPN-bacteria interaction using SEM and ζ-potential

Remarkable photodynamic antibacterial activity of **CPPN** toward Gram-positive and Gram-negative bacteria was further confirmed by observing the interactions of **CPPN** with bacteria using SEM imaging. We captured the SEM images of the treated and non-treated bacteria both in the dark and under light to observe the changes in their morphology. Figure 7a–c show the SEM images for treated and non-treated *E. coli*, *S. aureus*, and *B. subtilis* respectively, in both dark and light conditions. As shown in Figure 7a, when *E. coli* bacteria were treated with **CPPN** in the dark, the bacteria appeared to retain their shape and smooth surfaces without any noticeable damage. However, upon light irradiation for 10 min in the presence of **CPPN**, the morphology of *E. coli* changed completely. Therein, their membranes raptured and the cytoplasmic contents leaked out. For light control group without **CPPN**, the morphology of *E. coli* remained unchanged. These observations verified the important role of CPPN as a significant photosensitizer to produce ROS when it was irradiated with light. Similar phenomena have been observed in the case of treated and non-treated *S. aureus* and *B. subtilis* bacteria (Figure 7b,c).

To further study the interaction of CPPN with Gram-positive and Gram-negative bacteria, we performed ζ-potential measurements (Figure 7d). The three studied bacteria were treated with 20 μg ml^{-1} of **CPPN** in the dark and under white light irradiation for 10 min (22 mW cm^{-2}) and their ζ-potential values were then measured. Non-treated control groups of *E. coli*, *B. subtilis*, and *S. aureus* showed a ζ-potentials of −47.6, −36, and −30.6 mV, respectively, and upon treatment with **CPPN** in the dark, positive shifted values was seen for all the bacteria. The ζ-potential values drastically shifted to positive values for the bacteria treated with **CPPN** and irradiated with light for 10 min. These results indicate the interactions between **CPPN** and the three studied bacteria. Therein, *E. coli* experienced more positive shift in the ζ-potential value compared to *B. subtilis* and *S. aureus*. This can be attributed to the more negatively charged surface of *E. coli* as Gram-negative bacteria compared to the Gram-positive bacteria, *B. subtilis* and *S. aureus*.

2.5 | Mammalian cell cytotoxicity of CPPN

In order to investigate the effect of **CPPN** in terms of PDT in cancer research, cytotoxicity of **CPPN** was tested

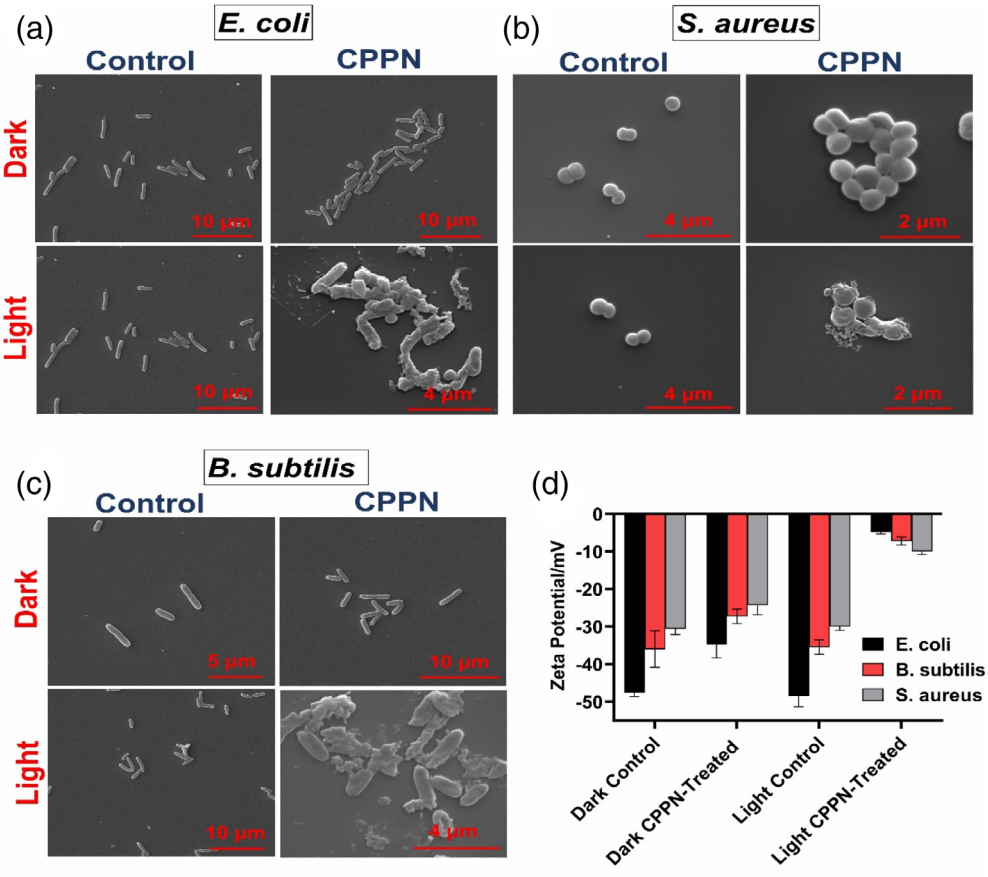

FIGURE 7 SEM images of (a) *E. coli*, (b) *S. aureus*, and (c) *B. subtilis* treated with **CPPN** and ampicillin in the dark and under white light irradiation (22 mW cm^{-2}) for 10 min, (d) ζ-potentials of the bacteria for control and **CPPN** treated samples in the dark and under white light irradiation for 10 min [Color figure can be viewed at wileyonlinelibrary.com]

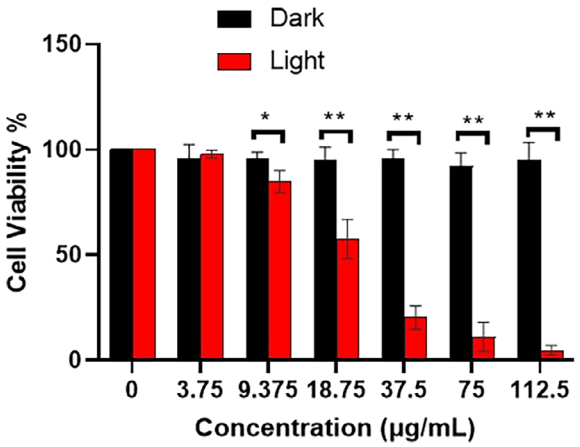

FIGURE 8 Relative cell viability (%) of **CPPN** against MCF-7 breast cancer cells at different concentrations in the dark and under light illumination (22 mW cm^{-2}, 20 min). 2-way ANOVA multiple comparison test was performed to compare results for the significant differences between groups. The data are represented as the mean ± SD ($n = 4$) (* and ** indicate a significant difference between groups with $p < 0.05$ and $p < 0.0001$, respectively) [Color figure can be viewed at wileyonlinelibrary.com]

using MTT assay on MCF-7 breast cancer cells. The cells were treated with various concentration of **CPPN** in the range of 3.75–112.5 μg ml^{-1}. Treated cells were compared with the control group which was nontreated cells that were accepted as having 100% cell viability in calculations (Figure 8). The cell viability difference between cell control and **CPPN** treated cells was nonsignificant in the dark. On the other hand, cells that were exposed to white light (20 mW cm^{-2}) for 20 min showed drastic decrease in cell viability. Nanoparticles exhibit a dose-dependent cytotoxicity against the MCF-7 cells. Around 55% of the cells were viable at a concentration of 18.75 μg ml^{-1}. A half maximal inhibitory concentration value (IC50) of white light exposed cells was determined as approximately 20.8 μg ml^{-1}. These findings explicitly demonstrated that, even at low concentrations, white light activates **CPPN** effectively, resulting in a substantial decrease in cell viability. It is a very powerful photosensitizer, with negligible cytotoxicity in the dark but high toxicity upon short time exposure to low intensity white light. These results support the findings in the antibacterial assays suggesting that **CPPN** is an ideal photosensitizer with negligible dark cytotoxicity.

3 | CONCLUSIONS

A new cross-linked conjugated polymer-porphyrin nanoparticle (**CPPN**) was successfully synthesized through CB6-AAC reaction of **CP-AZ** and **TPP-4AL** and it was fully characterized. **CP-AZ** was synthesized by Pd-catalyzed Suzuki cross-coupling reaction between 2,1,3-benzothiadiazole-4,7-bis (boronic acid pinacol ester) and the as-synthesized M3 monomer, 3-(2-azidoethyl)-2,-5-dibromothiophene monomer. **CPPN** was stable in aqueous medium without aggregation. Owing to its good light-triggered ROS generation ability even under lowfluence of white light and short exposure time, **CPPN** exhibited high biocidal activity against Gram-negative and Gram-positive bacteria as well as high cytotoxicity toward MCF-7 breast cancer cell line. Due to its negligible dark cytotoxicity, **CPPN** can be served as a promising therapeutic agent in light-induced antibacterial and anti-cancer therapies.

4 | EXPERIMENTAL SECTION

Experimental details on materials, characterization methods, reactive oxygen species (ROS) measurement, preparation of the bacterial suspension, minimum inhibitory concentration (MIC) assay, evaluation of the antibacterial activity of CPPN by surface plating method, preparation of treated bacteria samples for SEM imaging, evaluation of the antibacterial activity of CPPN by agar disk diffusion assay, in vitro cell viability assay, were given in the Supporting Information.

4.1 | Synthesis of 3-(2-azidoethyl)-2,5-dibromothiophene (M3)

2-(2,5-dibromothiophen-3-yl)ethan-l-ol (**M1**) and 2,5-dibromo-3-(2-bromoethyl)thiophene (**M2**) were synthesized following the literature procedures.[13] To a stirred solution of **M2** (585 mg, 1.68 mmol) in 7 ml DMSO, NaN_3 (273 mg, 4.2 mmol) was added. The reaction mixture was stirred at RT for 72 h. Then, 50 ml water was added to the reaction flask and followed by the extraction of the product with chloroform (3 × 50 ml). The organic phases were combined, and solvent was removed under reduced pressure to obtain a yellowish oil. Yield: 480 mg, 92%.

^{1}H NMR (400 MHz, $CDCl_3$, 25°C) δ (ppm): 2.82 (t, 2 H), 3.46 (t, 2 H), 6.85 (s, 1 H); ^{13}C NMR (100 MHz, $CDCl_3$, 25°C) δ (ppm): 29.7, 51.0, 109.1, 113.5, 132.4, 137.9.

4.2 | Synthesis of azide-functionalized conjugated polymer (CP-AZ)

M3 (585 mg, 1.88 mmol) and 2,1,3-benzothiadiazole-4,7-bis (boronic acid pinacol ester) (730 mg, 1.88 mmol) were placed in a two-necked round bottomed flask. Degassed THF (25 ml) and toluene (10 ml) were added

into the flask and the reaction mixture was stirred for 10 min under N_2(g). Then, 2 ml aqueous solution of K_2CO_3 (1.3 g, 9.4 mmol) was added followed by catalytic amount of tetrabutylammonium bromide (TBAB) (0.2 mmol). The reaction mixture was stirred for further 10 min followed by two freeze pump-thaw cycles to evacuate the flask and then the flask was filled with N_2(g). Then, catalytic amount of tetrakis(triphenylphosphine) palladium(0) (0.2 mmol) was added and the mixture was heated at 55°C while stirring for 72 h under N_2(g). When the reaction was over, the solvent was removed under reduced pressure to obtain solid residue which was washed with water several times. The precipitate was dissolved in minimum amount of THF and the solution was precipitated into cold methanol. Precipitates were collected by filtration and washed with MeOH several times. The product was finally dried under vacuum to give **CP-AZ** as reddish-brown powder. Yield: 439 mg, 82%.

^{1}H NMR (400 MHz, $CDCl_3$, 25°C) δ (ppm): 3.11 (m, 2 H), 3.46 (m, 2 H), 7.67–8.55 (m, 3 H); ^{13}C NMR (100 MHz, $CDCl_3$, 25°C) δ (ppm): 29.1–30.9, 50.7–51.4, 125.3–131.7, 135.8–140.0, 152.3–154.2.

4.3 | Synthesis of CPPN

CPPN was synthesized modifying our previously reported procedure.[10b] To a stirred solution of **CB6** (1.74 mg, 1.75×10^{-3} mmol) in 0.1 M HCl, **TPP-4AL** (0.5 mg, 4.9×10^{-4} mmol) was added. The solution was stirred for 15 min and the volume was made up to 200 ml with deionized water. Subsequently, a solution of **CP-AZ** (2 mg, 7×10^{-3} mmol) in 4 ml of THF was injected rapidly to the above solution under vigorous stirring. The mixture was sonicated for 1 h at RT and then it was left for overnight under ambient conditions. Then, the mixture was concentrated to the required volume and dialyzed against water using a 14 kDa MWCO regenerated cellulose membrane for 16 h to remove unreacted **CB6** and **TPP-4AL**.

ORCID

Dönüs Tuncel https://orcid.org/0000-0001-7762-9200

REFERENCES

[1] WHO (a), https://www.who.int/news-room/fact-sheets/detail/antimicrobial-resistance. (b) A. Petchiappan, D. Chatterji, *ACS Omega* **2017**, *2*, 7400. (c) P. Vikesland, E. Garner, S. Gupta, S. Kang, A. Maile-Moskowitz, N. Zhu, *Acc. Chem. Res.* **2019**, *52*, 916. (d) G. D. Wright, *Chem. Commun.* **2011**, *47*, 4055.

[2] (a) T. Maisch, *Photochem. Photobiol. Sci.* **2015**, *14*, 1518. (b) T. Maisch, *Mini Rev. Med. Chem.* **2009**, *9*, 974. (c) B. C. Wilson, M. S. Patterson, *Phys. Med. Biol.* **2008**, *53*, R61.

[3] (a) X. Zhao, J. Liu, J. Fan, H. Chao, X. Peng, *Chem. Soc. Rev.* **2021**, *50*, 4185. (b) Z. Zhou, J. Song, L. Nie, X. Chen, *Chem. Soc. Rev.* **2016**, *45*, 6597.

[4] (a) E. D. Sternberg, D. Dolphin, C. Brückner, *Tetrahedron* **1998**, *54*, 4151. (b) M. Ethirajan, Y. Chen, P. Joshi, R. K. Pandey, *Chem. Soc. Rev.* **2011**, *40*, 340. (c) M. Rajora, J. Lou, G. Zheng, *Chem. Soc. Rev.* **2017**, *46*, 6433.

[5] (a) S. Singh, A. Aggarwal, N. D. K. Bhupathiraju, G. Arianna, K. Tiwari, C. M. Drain, *Chem. Rev.* **2015**, *115*, 10261. (b) X. Li, S. Lee, J. Yoon, *Chem. Soc. Rev.* **2018**, *47*, 1174.

[6] (a) A. Gupta, S. Mumtaz, C.-H. Li, I. Hussain, V. M. Rotello, *Chem. Soc. Rev.* **2019**, *48*, 415. (b) X. Li, H. Bai, Y. Yang, J. Yoon, S. Wang, X. Zhang, *Adv. Mater.* **2019**, *31*, 1805092. (c) L. Zhou, T. Qiu, F. Lv, L. Liu, J. Ying, S. Wang, *Adv. Healthcare Mater.* **2018**, *7*, 1800670.

[7] (a) J. Li, K. Pu, *Chem. Soc. Rev.* **2019**, *48*, 38. (b) Y. Jiang, K. Pu, *Acc. Chem. Res.* **2018**, *51*, 1840. (c) D. Cui, J. Huang, X. Zhen, J. Li, Y. Jiang, K. Pu, *Am. Ethnol.* **2019**, *58*, 5920. (d) Z. H. Yu, X. Li, F. Xu, X. L. Hu, J. Yan, N. Kwon, G. R. Chen, T. Tang, X. Dong, Y. Mai, *Am. Ethnol.* **2020**, *132*, 3687. (e) B. Wang, G. Feng, M. Seifrid, M. Wang, B. Liu, G. C. Bazan, *Am. Ethnol.* **2017**, *56*, 16063. (f) D. Tuncel, H. V. Demir, *Nanoscale* **2010**, *2*, 484. (g) D. Tuncel, *Nanoscale Adv.* **2019**, *1*, 19. (h) G. Feng, Y. Fang, J. Liu, J. Geng, D. Ding, B. Liu, *Small* **2017**, *13*, 1602807. (i) Y. Wang, S. Li, L. Liu, L. Feng, *ACS Appl. Bio Mater.* **2018**, *1*, 27. (j) J. Pennakalathil, E. Jahja, E. S. Özdemir, O. Konu, D. Tuncel, *Biomacromolecules* **2014**, *15*, 3366.

[8] (a) D. Tuncel, J. H. Steinke, *Macromolecules* **2004**, *37*, 288. (b) D. Tuncel, H. B. Tiftik, B. Salih, *J. Mater. Chem.* **2006**, *16*, 3291. (c) D. Tuncel, Ö. Özsar, H. B. Tiftik, B. Salih, *Chem. Commun.* **2007**, 1369. (d) D. Tuncel, Ö. Ünal, M. Artar, *Isr. J. Chem.* **2011**, *51*, 525. (e) D. Tuncel, N. Cindir, Ü. Koldemir, *J. Inclusion Phenom. Macrocyclic Chem.* **2006**, *55*, 373. (f) M. Özkan, Y. Keser, S. E. Hadi, D. Tuncel, *Eur. J. Org. Chem.* **2019**, *2019*, 3534.

[9] K. Kim, *Cucurbiturils and Related Macrocycles*, Royal Society of Chemistry, Cambridge **2019**.

[10] (a) D. Tuncel, *Cucurbituril-based Functional Materials*, Royal Society of Chemistry, Cambridge **2019**. (b) V. Ibrahimova, S. Ekiz, Ö. Gezici, D. Tuncel, *Polym. Chem.* **2011**, *2*, 2818. (c) M. Özkan, Y. Kumar, Y. Keser, S. E. Hadi, D. N. S. Tuncel, *ACS Appl. Bio Mater.* **2019**, *2*, 4693. (d) M. Özkan, Y. Keser, A. Koc, D. Tuncel, *J. Porphyr. Phthalocyanines* **2019**, *23*, 1406. (e) L. Chen, H. Bai, J.-F. Xu, S. Wang, X. Zhang, *ACS Appl. Mater. Interfaces* **2017**, *9*, 13950. (f) K. Liu, Y. Liu, Y. Yao, H. Yuan, S. Wang, Z. Wang, X. Zhang, *Am. Ethnol.* **2013**, *52*, 8285. (g) A. C. Bhasikuttan, H. Pal, J. Mohanty, *Chem. Commun.* **2011**, *47*, 9959. (h) K. M. Park, K. Suh, H. Jung, D.-W. Lee, Y. Ahn, J. Kim, K. Baek, K. Kim, *Chem. Commun.* **2009**, 71. (i) A. Koc, R. Khan, D. Tuncel, *Chem. – Eur. J.* **2018**, *24*, 15550. (j) Y. Kumar, B. Patil, A. Khaligh, S. E. Hadi, T. Uyar, D. Tuncel, *ChemCatChem* **2019**, *11*, 2994.

[11] X. Tian, Z. Zhao, D. Li, B. Zhang, Y. Chen, *Org. Electron.* **2019**, *69*, 153.

[12] G. A. Pankuch, G. Lin, D. B. Hoellman, C. E. Good, M. R. Jacobs, P. C. Appelbaum, *Antimicrob. Agents Chemother.* **2006**, *50*, 1727.

[13] J. Pennakalathil, A. Özgün, I. Durmaz, R. Cetin-Atalay, D. Tuncel, *J. Polym. Sci. Polym. Chem.* **2015**, *53*, 114.

SUPPORTING INFORMATION

Additional supporting information may be found in the online version of the article at the publisher's website.

How to cite this article: I. K. Duah, A. Khaligh, A. Koç, D. D. A. Başaran, D. Tuncel, *J. Appl. Polym. Sci.* **2021**, e51777. https://doi.org/10.1002/app.51777